Supplementary

Designing Descriptor for the Computational Screening of Argyrodite-based Solid-State Superionic Conductors: Uniformity of Ion-Cage Size

Byeongsun Jun[1] and Sang Uck Lee[1,2*]

[1]*Department of Bionano Technology, Hanyang University, Ansan, 15588, Republic of Korea.*

[2]*Department of Applied Chemistry, Center for Bionano Intelligence Education and Research, Hanyang University, Ansan 15588, Republic of Korea.*

*Corresponding authors Email: sulee@hanyang.ac.kr (Sang Uck Lee)

Keywords: Argyrodite, Solid electrolyte, AIMD, Li-ion conductivity, Site disorder, Ion cage

Section A: Theoretical Background of Li-ion Conductivity Calculation

Molecular dynamics (MD) simulations calculate the behavior of atoms by integrating the Newtonian equations for the interactions between atoms at a finite temperature.[1, 2] Interactions between atoms are either fitted in an experiment called a force field or calculated using a predefined potential from first principal calculations. This method can be adopted even for large systems with few computational resources, but if there is no suitable force field that can analyze the material to be studied, accurate calculations cannot be performed. On the other hand, *ab initio* molecular dynamics simulations (AIMD) calculate the interactions between atoms by solving Schrödinger's equation, so any new material can be accurately calculated theoretically.[3, 4] Another advantage of AIMD is that it interprets the mechanism of ionic diffusion by analyzing the trajectory of the atom by dynamics, unlike the nudged elastic band (NEB)[5] method. The NEB method is useful when calculating the energy barrier required for the movement of an atom, but it is limited in its use because it is difficult to define the movement path of mobile ions for materials where concerted motion occurs, such as a super ionic conductor. Recently, the mechanism for ionic diffusion in a super ionic conductor has been successfully identified using AIMD simulations.[6-8] AIMD simulations clearly have a drawback in that they require a considerable amount of computation time compared to classical MD or NEB calculations. Therefore, it is necessary to determine a reasonable criterion that can effectively express ionic diffusion. Several critical factors to consider when calculating ionic conductivity of solid-state electrolytes with AIMD simulations are described below.

Simulation cell size and configuration generation

As the size of the supercell increases, the accuracy of the simulation improves, but the calculation time increases exponentially. To reduce the amount of calculation time, the minimum size should be selected without distortion due to periodic boundary. In general, the

size of each lattice constant is at least 10Å, but for accurate calculation, it is necessary to increase the size of the supercell and check that there is a convincing difference from the smaller size results.

Argyrodite has a unique property that the ionic conductivity depends on the site disorder of single anions (S^{2-} and X^{-}) at 4a and 4c sites. There are six possible configurations of site disorder, and each configuration has a different structural stability and ionic conductivity. In addition, Li sites are not fully occupied in crystallographic sites. Therefore, we generated unique configurations using 'enumlib' code (https://github.com/msg-byu/enumlib) [9-12] which generates the derivate symmetry distinct superstructures of a parent lattice. In the case of Li_6PS_5Cl, we extract all available symmetry distinct combinations when four S^{2-} and four Cl^{-} are distributed at the 4a and 4c sites by assuming that 24 Li^{+} are fully occupied at the 24g sites because 24g site is the center of 48h sites as shown in Figure 1(a). Here, we obtained 6 highly symmetric cubic structures as listed in Table 1 and Table S3. From the same perspective, we generated the halogen excess $Li_{5.75}PS_{4.75}Cl_{1.25}$ configurations when three S^{2-} and five Cl^{-} occupied the 4a and 4c sites, and at the same time. However, the difference here is that one Li^{+} must be removed from the 24g sites for the charge neutrality because S^{2-} is replaced by Cl^{-}. So, we used 'enumlib' code to find Li^{+} distribution configurations, among the constructed configurations [23, 114 and 211 configurations for each $Li_{5.75}PS_{4.75}Cl_{1.25}$, $Li_5PS_{4.5}Cl_{1.5}$, and $Li_{5.25}PS_{4.25}Cl_{1.75}$], we selected the most stable configuration through full relaxation calculations.

Simulation temperatures

To reduce the simulation time, it is common to perform AIMD simulations at a high temperature (500 K to 2000 K) with enough diffusion. However, if melting of the crystal structure is observed during simulation, it should be carried out at a lower temperature. Usually, the melting point of sulfides is less than 1200 K, and oxides have a higher melting point. In the

case of a material whose ionic behavior changes due to a phase transition (due to temperature), it is necessary to be careful because fitting using a high temperature simulation result may not be effective at low temperature. A larger number of simulated temperatures results in more accurate fitting, but in this study, we considered 5 or 6 temperatures from 600K to 1200K to reduce the computational cost.

Total simulation time and convergence criteria of AIMD simulations

Sufficient simulation time is required to observe necessary ion migration for ionic conductivity calculation, but the AIMD simulation must be terminated within a reasonable simulation time because the simulation cannot be continued indefinitely. So, the Mo group proposed an appropriate criterion for the simulation called the relative standard deviation (RSD) of the ionic conductivity and the effective number of ion hops.[13] We monitored RSD values during AIMD simulations and stopped the simulations when the criteria were met (RSD < 0.25 with total effective ion hops greater than 250). In the case of Li-argyrodite with disordered anion sites, nearly 100 ps at 800 K is required to meet the criteria mentioned above. On the other hand, the anion site ordered structure requires a simulation time of 500 ps or more at 800 K.

Ionic conductivity

The diffusivity (D) can be obtained from fitting of the mean square displacement (MSD) versus $2dt$ by calculating the movement of mobile ions per time from trajectories generated as a result of AIMD simulations.

$$D = \frac{1}{2dt}\mathrm{MSD} \tag{1}$$

The MSD of mobile ions can be calculated from the average displacements over time duration t, where $r_i(t)$ is the position of a mobile ion.

$$\mathrm{MSD} = \frac{1}{N}\sum_i \langle [r_i(t+t_0)]^2 - [r_i(t_0)]^2 \rangle \quad (2)$$

Generally, diffusivity follows an Arrhenius relationship when there is no phase transition in the corresponding temperature range:

$$D = D_0 \exp\left(-\frac{E_a}{kT}\right) \quad (3)$$

Here, D_0 is the diffusivity at infinite temperature, E_a is the activation energy of diffusion, k is the Boltzmann constant and T is temperature. E_a can be obtained from a linear fitting of the *log(D)* versus $1/T$. Since the AIMD simulations are performed at high temperatures with many diffusion events, D at a low temperature (room temperature) is extrapolated from **Eqn. (3)**. Then, ionic conductivity (σ) can be calculated from the Nernst-Einstein relation:

$$\sigma_{\mathrm{T}} = \frac{\rho z^2 F^2}{RT} D_{\mathrm{T}} \quad (4)$$

where ρ is the molar density of mobile ions in the unit cell, and F, R and z are Faraday's constant, the gas constant, and the charge of mobile ions, respectively.

Ensemble average

To satisfy the ergodicity, we performed AIMD simulations at least three times with the same structure and temperature. The final ionic conductivity is calculated as the average of the ionic conductivities extrapolated to room temperature in all simulations.

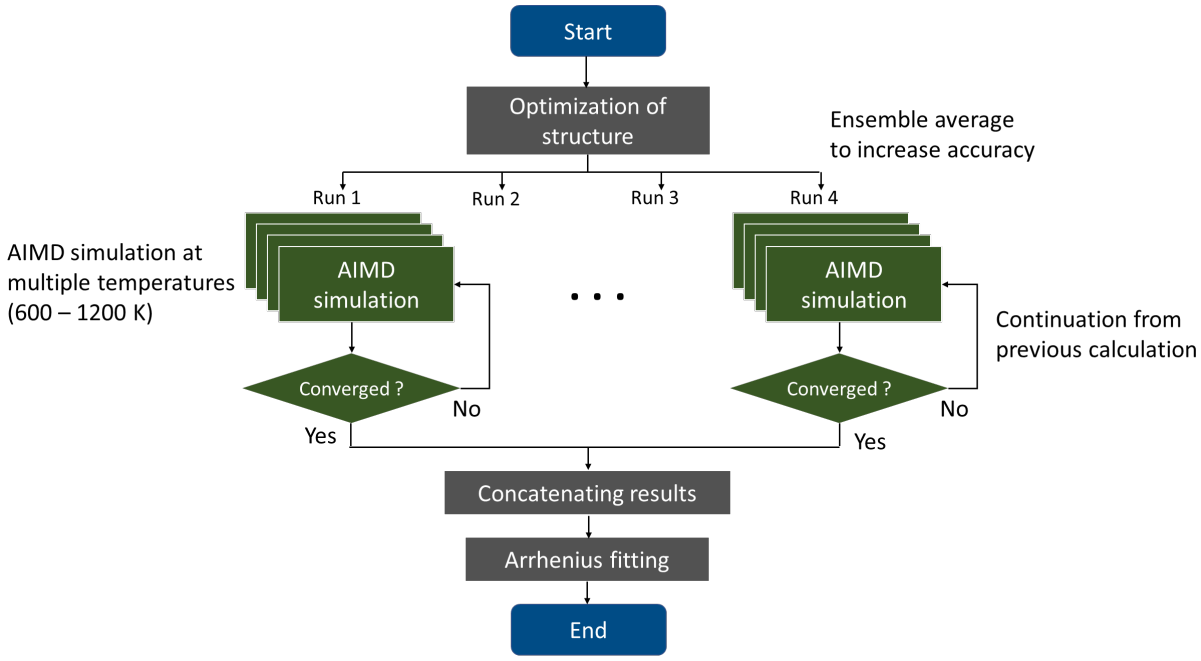

Figure S1. Schematic workflow of AIMD simulations to obtain ionic conductivity (σ_{RT}) at room temperature. After structural optimization, an independent full simulation is performed at multiple temperatures. Finally, results are concatenated by ensemble average and σ_{RT} is obtained using Arrhenius fitting.

Analysis methods

The diffusion information associated with the ion conductor can be obtained by analyzing the trajectory obtained as a result of the AIMD simulations. The probability density function P(r) can be obtained by creating a three-dimensional grid of the unit cell crystal structure, calculating the number of diffusion ions during the simulation time, and then normalizing it to the volume.[14] In an ion conductor, the density of ions appears high at low energy positions, and the locations where the isosurface is connected can be interpreted as diffusion paths. The correlation information of ion diffusion can be analyzed using the van Hove distribution function.[15] The van Hove distribution function is defined as the probability

of ions moving r from their original position during a given time t and it can usually be separated into a self-part (G_s) and a distinct-part (G_d) as follows:

$$G(r,t) = \frac{1}{N}\left\langle \sum_{i=1}^{N} \delta\big(r + r_i(0) - r_i(t)\big) \right\rangle + \frac{1}{N}\left\langle \sum_{i \neq j}^{N} \delta\left(r + r_j(0) - r_i(t)\right) \right\rangle$$

$$\equiv G_s(r,t) + G_d(r,t) \tag{5}$$

Here, $\langle \cdot \rangle$ is an ensemble average and $\delta(\cdot)$ is the three-dimensional Dirac delta function. G_s represents the distance traveled by the ion from its initial position after time t has elapsed. Therefore, if a strong peak appears at the same distance for a long time, the ion diffusion does not happen properly. G_d provides information on the movement of the remaining N-1 ions, and it can be seen how fast the reference ion site is replaced with other ions. In this study, the probability density function and van Hove correlation function were obtained using pymatgen-diffusion code implemented on pymatgen.[16, 17]

Section B: Li-ion conductivity correction

Bulk Ionic Conductivity of Li-argyrodite

Argyrodite has a unique property that the ionic conductivity depends on the site disorder of single anions (S^{2-} and X^{-}) at 4a and 4c sites. There are six possible configurations of site disorder, and each configuration has a different structural stability and ionic conductivity. Therefore, the bulk ionic conductivity is represented as different contributions of each configuration depending on the relative stability and ionic conductivity, as shown in Figure S2. The thermodynamically more stable configuration accounts for most of the argyrodite structure, contributing more to the bulk ionic conductivity. In addition, the configuration with the lowest ionic conductivity would reasonably be expected to have a significant impact on bulk ionic conductivity, acting as a bottleneck region for ion diffusion. The Li-ion diffusion through the bulk argyrodite is limited by the slowest diffusion region, not the fastest diffusion region. Consequently, we devised a method to evaluate the bulk ionic conductivity considering both thermodynamic and kinetic effects.

The thermodynamic ($P_i(E)$) and kinetic ($P_i(\sigma)$) contribution of each configuration to the bulk ionic conductivity can be described by the Boltzmann distribution function:

$$P_i(E) \propto e^{\frac{-\Delta E}{kT}} \tag{6}$$

$$P_i(\sigma) \propto e^{\frac{-\Delta \sigma}{kT}} \tag{7}$$

where ΔE represents relative stability compared to the most stable configuration, $\Delta\sigma$ is the relative ionic conductivity compared to the lowest ionic conductivity among ionic conductivities of all configurations, and k and T are the Boltzmann constant and temperature, respectively.

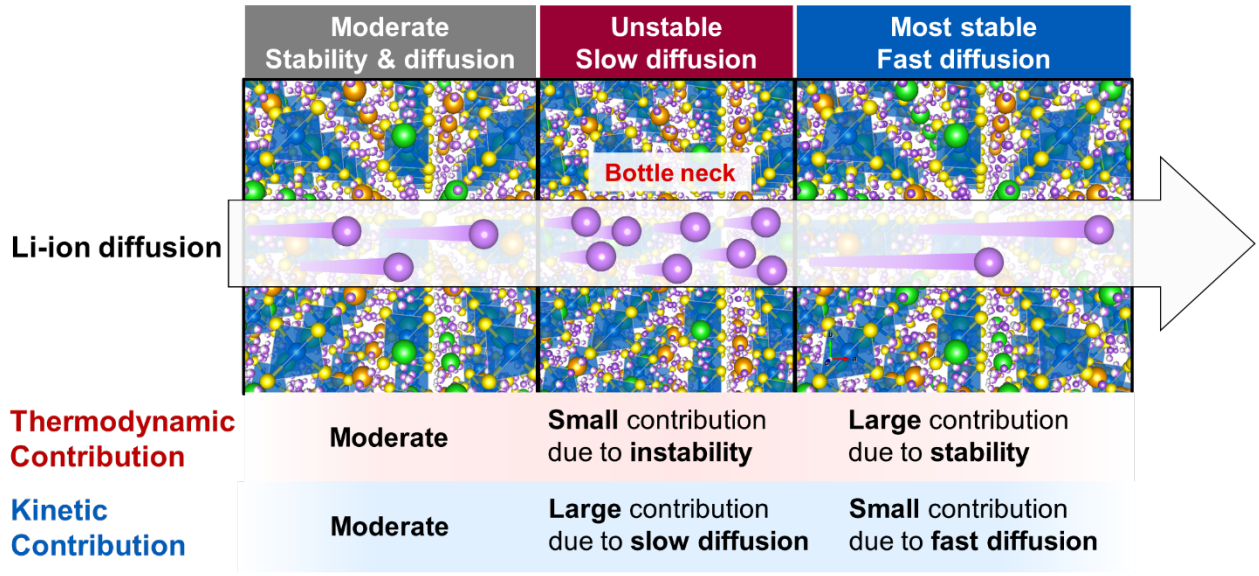

Figure S2. Schematic illustration of Li-ion diffusion in bulk Li_6PS_5Cl. The contribution of each configuration to bulk ionic conductivity depends on the relative thermodynamic structural stability and its own ionic conductivity.

Then, the total contribution of each configuration to the bulk ionic conductivity was calculated by multiplying thermodynamic ($P_i(E)$) and kinetic ($P_i(\sigma)$) contribution, $P_i = P_i(E)P_i(\sigma)$. Here, the distribution P_i is normalized so that the total sum of each P_i is 1. Finally, the bulk ionic conductivity is calculated by the following equation:

$$\sigma_{\text{bulk}} = \sum_i P_i \, \sigma_i \tag{8}$$

Table S1 shows a summary of the evaluation of bulk ionic conductivities including calculated relative stability, Li-ion conductivity of each configuration and their contributions to the bulk ionic conductivity ($P_i(E)$ and $P_i(\sigma)$) with the final bulk conductivity (σ_{bulk}) considering 100% crystallinity of Li_6PS_5Cl.

Table S1. Calculated relative stability (ΔE, in meV/atom) and Li-ion conductivity of each configuration (σ_{RT}, in mS/cm at 300K), the contribution of each configuration ($P_i(E)$ and $P_i(\sigma)$) to the bulk ionic conductivity, and the bulk conductivity (σ_{bulk}) considering 100% crystallinity of Li_6PS_5Cl.

Site occupancy (Cl^- @ 4c)	ΔE (meV/atom)	$\boldsymbol{P_i(E)}$	$\boldsymbol{P_i(\sigma)}$	$\boldsymbol{P_i(E)P_i(\sigma)}$ $\boldsymbol{P_i}$	Normalized $\boldsymbol{P_i}$	σ_{RT} (mS/cm)
0%	23	0.4121	1.0000	0.4121	0.6482	0.02
25%	4	0.8678	0.1739	0.1509	0.2373	45
50%	0	1.0000	0.0114	0.0114	0.0179	115
50%	11	0.6450	0.0028	0.0018	0.0029	183
75%	13	0.6107	0.0970	0.0592	0.0932	60
100%	206	0.0003	0.9795	0.0003	0.0005	0.57

$\sigma_{\text{bulk}} = \sum_i P_i \, \sigma_i = 18.79$ mS/cm

Crystallinity of Li-argyrodite

Even if various physical properties are obtained with an accurate calculation method, there will be differences in results due to differences in the experimental environment. In particular, the inevitable difference is that the theoretically designed crystal structure is a perfect crystal without any defects, unlike the synthesized material. In recent theoretical research on solid-state electrolytes, it has been reported that there is a difference between the experimentally measured Li-ion conductivity and the theoretical calculation results due to the unique properties of the crystal structure.[18, 19] Argyrodite also has a unique Li-ion diffusion mechanism called inter-cage diffusion, and the crystallinity of argyrodite is expected to have a significant effect on Li-ion diffusion. From this point of view, it has recently been reported that $Li_{6-x}PS_{5-x}Cl_{1+x}$ of various compositions was synthesized by various methods and the effect on Li-ion conductivity was studied by quantitatively measuring crystallinity.[20] We compared the experimentally measured crystallinity and Li-ion conductivity of various compositions of $Li_{6-x}PS_{5-x}Cl_{1+x}$ with the theoretical Li-ion conductivity assuming perfect crystals to obtain a regression analysis relation, $\sigma_{exp.} = \sigma_{calc.}\chi_c^{7.14}$, as shown in Figure 3(a). Here, $\sigma_{exp.}$ and $\sigma_{calc.}$ are the experimental and calculated Li-ion conductivity, and χ_c is the degree of crystallinity. The regression equation shows that most of the ionic conductivities reported in the literature correspond to crystallinity values between 70% and 80%, Figure S3(b) and Table S2. Therefore, in this study, we used the calculated Li-ion conductivity reflecting 80% crystallinity. Applying this idea, our calculations can provide the maximum Li-ion conductivity that can be derived experimentally.

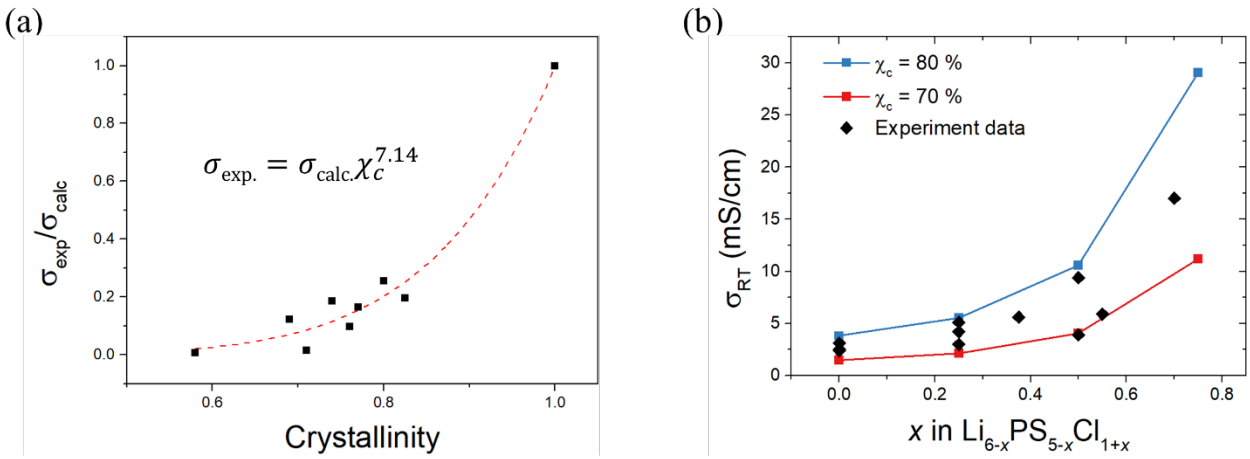

Figure S3. (a) Scatter plot with regression curve of $\sigma_{exp.}/\sigma_{calc.}$ with respect to experimentally measured crystallinity of argyrodite $Li_{6-x}PS_{5-x}Cl_{1+x}$. $\sigma_{exp.}$ and $\sigma_{calc.}$ are experimental and calculated ionic conductivities, and χ_c is the degree of crystallinity. The inset is the regression equation. (b) Comparison between the calculated Li-ion conductivity of argyrodite $Li_{6-x}PS_{5-x}Cl_{1+x}$ at 80% and 70% crystallinity and experimentally measured Li-ion conductivities.

Table S2. Calculated Li-ion conductivity of argyrodite $Li_{6-x}PS_{5-x}Cl_{1+x}$ at 100%, 80% and 70% crystallinity with experimental results.

x in $Li_{6-x}PS_{5-x}Cl_{1+x}$	Calculated (mS/cm)			Experiment (mS/cm)
	$\chi_c = 1.0$	$\chi_c = 0.8$	$\chi_c = 0.7$	
0	18.79	3.82	1.47	3.10[20], 2.30[20], 2.5[21]
0.25	27.32	5.55	2.14	7.00[20], 5.10[20], 4.2[21]
0.375	-	-	-	5.6[21]
0.5	52.11	10.59	4.08	10.20[20], 5.10[20], 12.0[21], 5.9[21]
0.7	-	-	-	17[22]
0.75	142.89	29.04	11.19	-

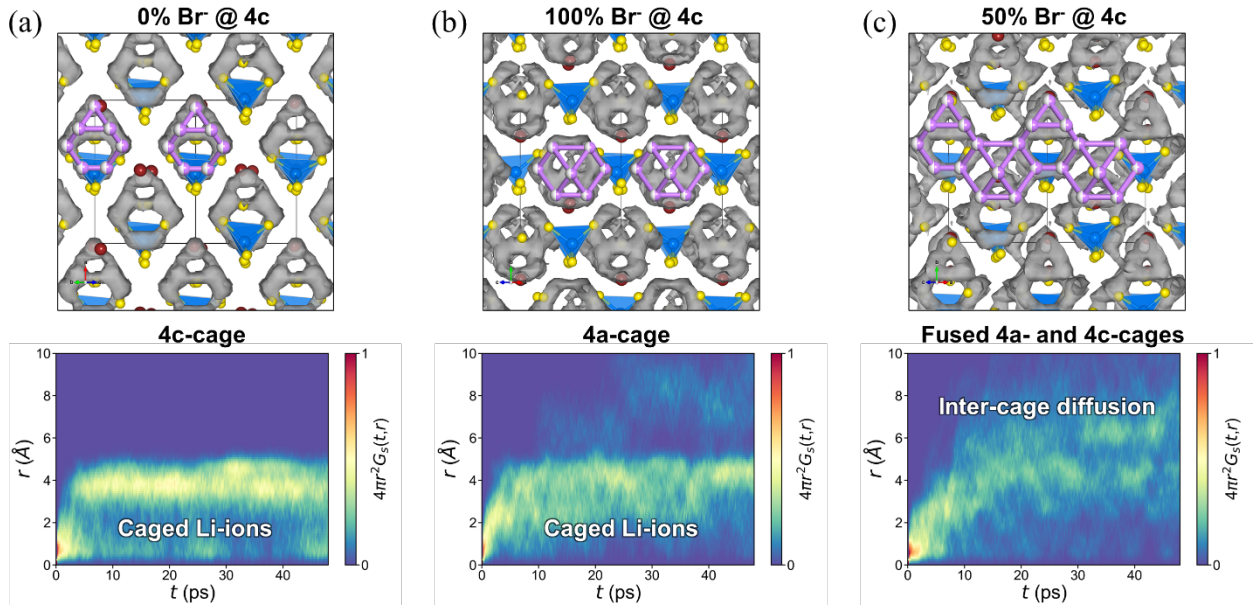

Figure S4. Isosurfaces of Li-ion probability density distribution (upper) and self-part of van Hove correlation function (lower) of Li_6PS_5Br for different site disorder configurations. 100% Br^- filled ordered configuration at (a) 4a site or (b) 4c sites, and (c) 50% site disordered configuration.

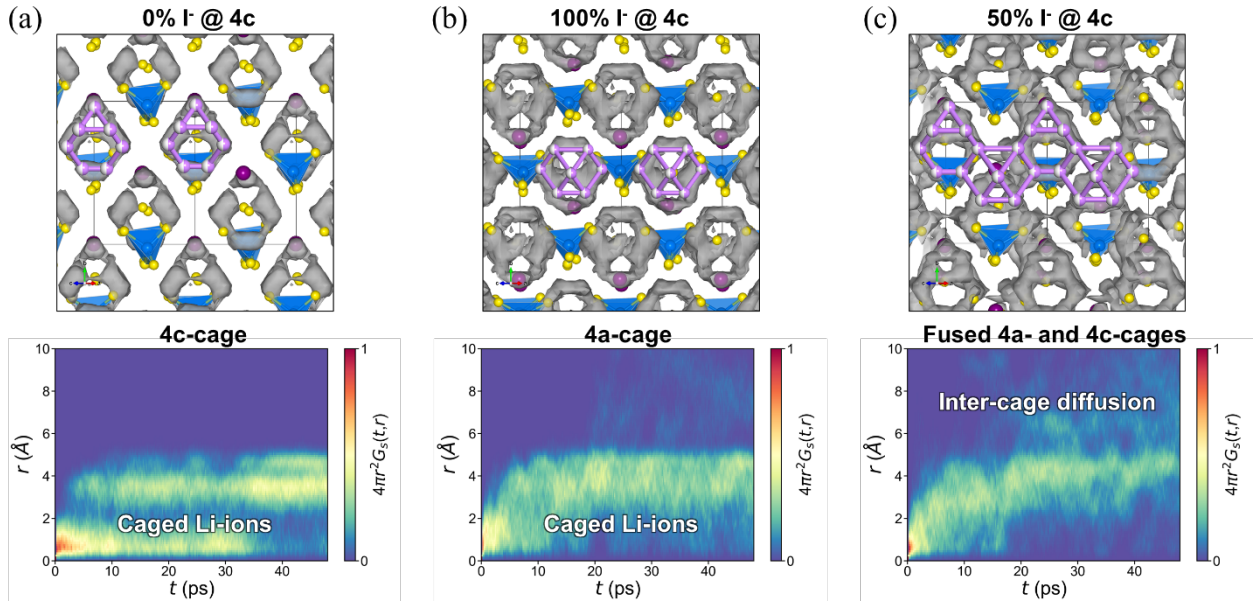

Figure S5. Isosurface of Li-ion probability density distribution (upper) and self-part of van Hove correlation function (lower) of Li_6PS_5I at different site disorder configurations. 100% I^- filled ordered configuration at (a) 4a site or (b) 4c sites, and (c) 50% site disordered configuration.

Table S3. Calculated relative stability (E_{rel}, in meV/atom), Li-cage size as radius, and Li ion conductivity at 300K with min-max fluctuations according to site disorder of S^{2-}/X^{-} single anions at 4a and 4c sites. Corrected Li-ion conductivity ($\sigma_{bulk}^{\chi_c}$)[a] of bulk $Li_{6-x}PS_{5-x}Cl_{1+x}$ was calculated using 80% crystallinity (χ_c).

$Li_{6-x}PS_{5-x}X_{1+x}$		Site occupancy				E_{rel}	Li cage radius (Å)				STD[b]	Conductivity (mS/cm) $\sigma^{0.8}[\sigma_{min}^{0.8},\ \sigma_{max}^{0.8}]$
		4a		4c			4a		4c			
		X^-	S^{2-}	X^-	S^{2-}		X^-	S^{2-}	X^-	S^{2-}		
Cl	0.25	100%	0%	25%	75%	2.7	2.68	-	2.47	2.42	0.1174	3.05 [2.24, 4.07]
		75%	25%	50%	50%	0.0	2.62	2.52	2.50	2.40	0.0885	10.57 [7.52, 14.84]
		50%	50%	75%	25%	8.4	2.51	2.54	2.54	2.44	0.0601	14.03 [10.77, 17.89]
		25%	75%	100%	0%	29.6	2.40	2.46	2.58	-	0.0817	14.43 [11.18, 18.50]
	0.5	100%	0%	50%	50%	8.5	2.65	-	2.50	2.42	0.0997	8.13 [6.10, 10.77]
		75%	25%	75%	25%	0.0	2.57	2.49	2.51	2.38	0.0814	13.01 [10.57, 15.85]
		50%	50%	100%	0%	7.8	2.48	2.47	2.54	-	0.0517	14.03 [11.18, 17.68]
	0.75	100%	0%	75%	25%	6.7	2.59	-	2.51	2.38	0.0894	28.25 [21.95, 36.79]
		75%	25%	100%	0%	0.0	2.52	2.47	2.50	0.00	0.0335	29.88 [20.94, 42.69]
Br	0.25	100%	0%	25%	75%	0.0	2.88	-	2.67	2.39	0.2085	1.04 [0.73, 1.46]
		75%	25%	50%	50%	0.5	2.74	2.75	2.63	2.40	0.1535	6.10 [4.88, 7.52]
		50%	50%	75%	25%	11.3	2.70	2.65	2.67	2.38	0.1391	13.21 [10.57, 16.67]
		25%	75%	100%	0%	18.6	2.57	2.68	2.66	-	0.0833	6.91 [5.49, 8.74]
	0.5	100%	0%	50%	50%	0.0	2.78	-	2.64	2.40	0.1617	4.88 [3.66, 6.50]
		75%	25%	75%	25%	6.3	2.70	2.72	2.62	2.42	0.1409	15.65 [11.59, 21.14]
		50%	50%	100%	0%	8.0	2.67	2.75	2.67	-	0.0674	8.74 [6.50, 11.79]
	0.75	100%	0%	75%	25%	0.9	2.74	-	2.62	2.40	0.1407	10.98 [9.15, 13.42]
		75%	25%	100%	0%	0.0	2.68	2.70	2.66	-	0.0646	19.51 [15.45, 24.80]

I	0.25	100%	0%	25%	75%	0.0	3.05	-	2.76	2.39	0.2703	0.0041 [0.0020, 0.0061]
		75%	25%	50%	50%	9.4	2.93	2.71	2.83	2.40	0.2131	4.47 [3.46, 5.69]
		50%	50%	75%	25%	20.1	2.85	2.63	2.83	2.39	0.1919	6.10 [4.07, 9.35]
		25%	75%	100%	0%	36.1	2.70	2.66	2.83	-	0.0896	2.03 [1.63, 2.44]
	0.5	100%	0%	50%	50%	0.0	2.95	-	2.79	2.38	0.2408	1.08 [0.83, 1.38]
		75%	25%	75%	25%	9.0	2.90	2.68	2.79	2.38	0.2182	5.69 [4.47, 6.91]
		50%	50%	100%	0%	13.8	2.84	2.65	2.85	-	0.1111	7.32 [5.28, 9.96]
	0.75	100%	0%	75%	25%	0.0	2.93	-	2.76	2.39	0.2282	5.89 [4.27, 8.13]
		75%	25%	100%	0%	8.2	2.85	2.59	2.81	-	0.1271	18.50 [13.01, 25.81]

[a] Details are described in Supporting Information Section B.

[b] Standard deviation of all Li-cage sizes.

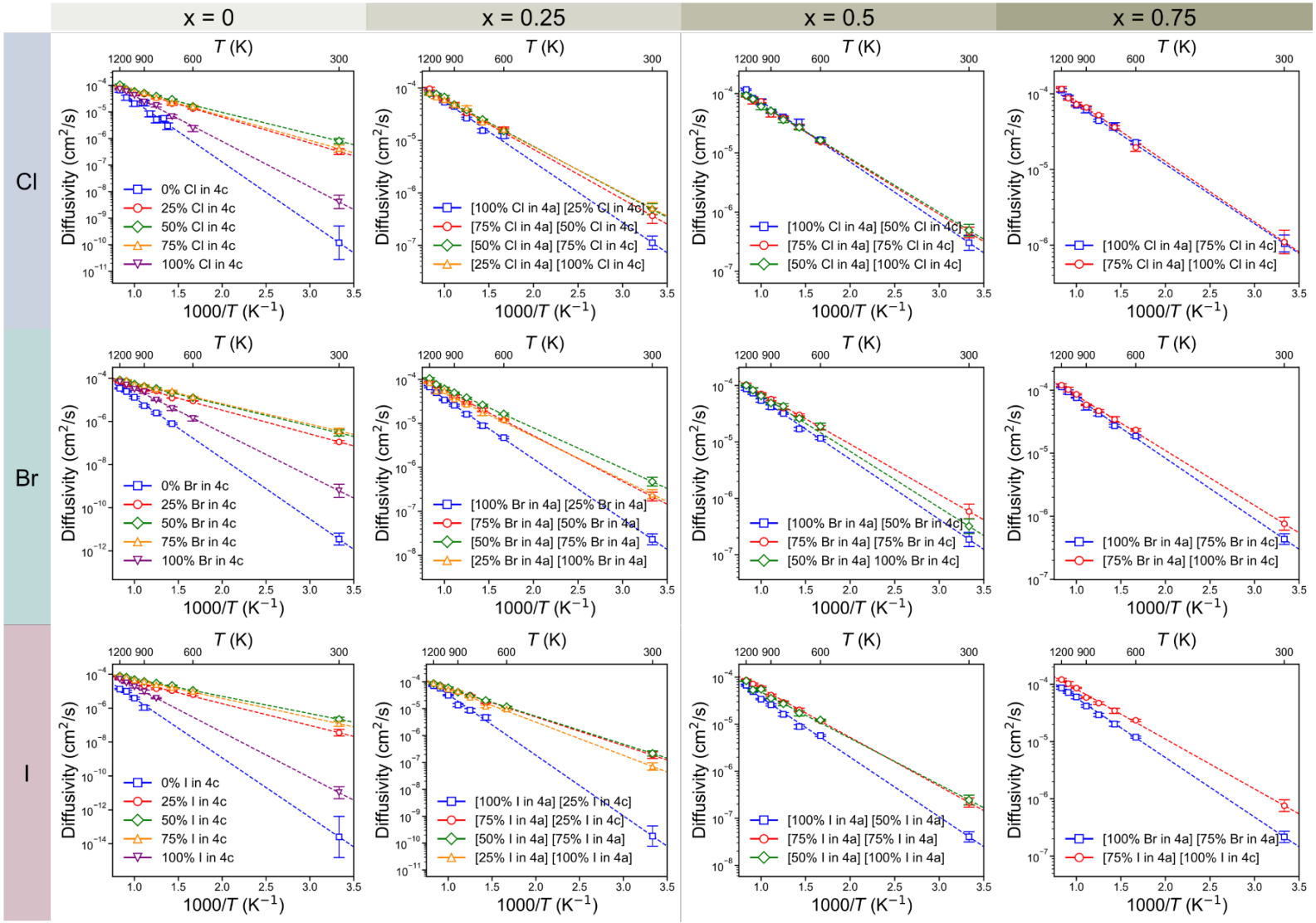

Figure S6. Arrhenius plots of diffusivities calculated by AIMD simulation of $Li_{6-x}PS_{5-x}X_{1+x}$ (x = 0, 0.25, 0.5, 0.75), X = (a) Cl, (b) Br and (c) I according to site disorder in the temperature range from 600 K to 1200 K for extrapolated diffusivity at 300 K.

Table S4. Calculated relative energies between LT and HT phases of argyrodite according to the halogen ratio.

Composition	Stable phase	ΔE_{LT-HT} (meV/atom)
Li_6PS_5Cl	HT	2.99
$Li_{6.25}PS_{5.25}Cl_{0.75}$	LT ~ HT	-0.56
$Li_{6.5}PS_{5.5}Cl_{0.5}$	LT	-1.99
$Li_{6.75}PS_{5.75}Cl_{0.25}$	LT	-6.29
Li_7PS_6	LT	-12.08

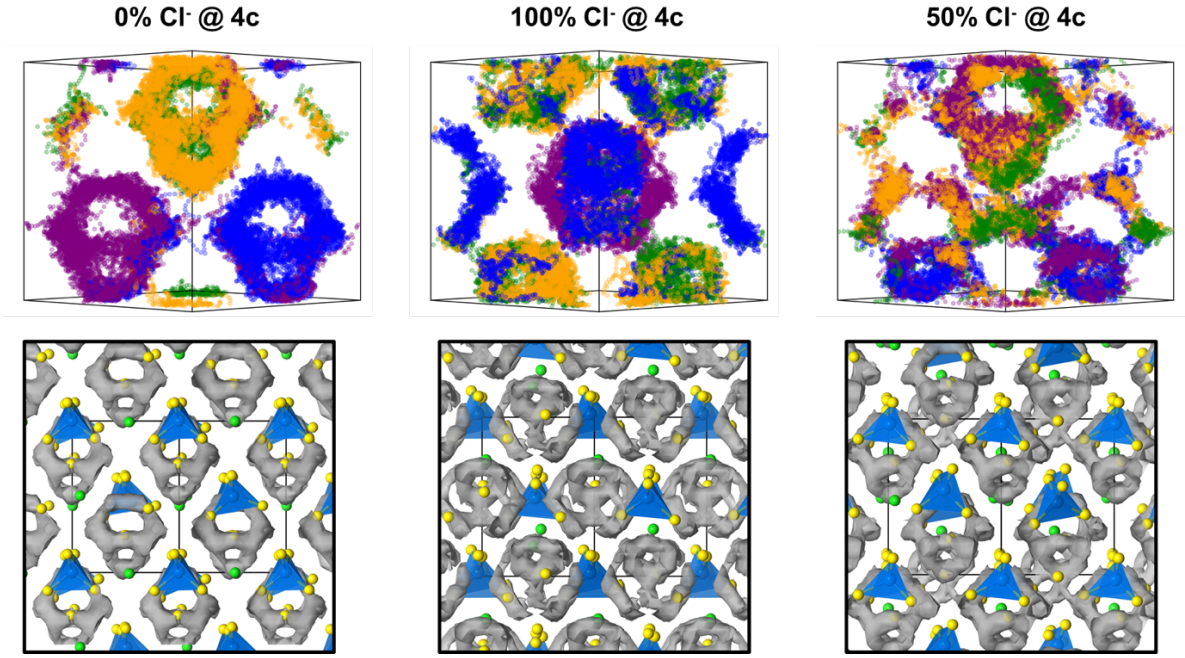

Figure S7. Li-ion trajectories and probability densities of Li-ion during 20ps AIMD simulations at 900K for different site disorder configurations of Li_6PS_5Cl, 100% Cl^- filled ordered configuration at 4a- or 4c-sites and 50% site disordered configuration. Each color of the Li-ion trajectory indicates different Li-ion.

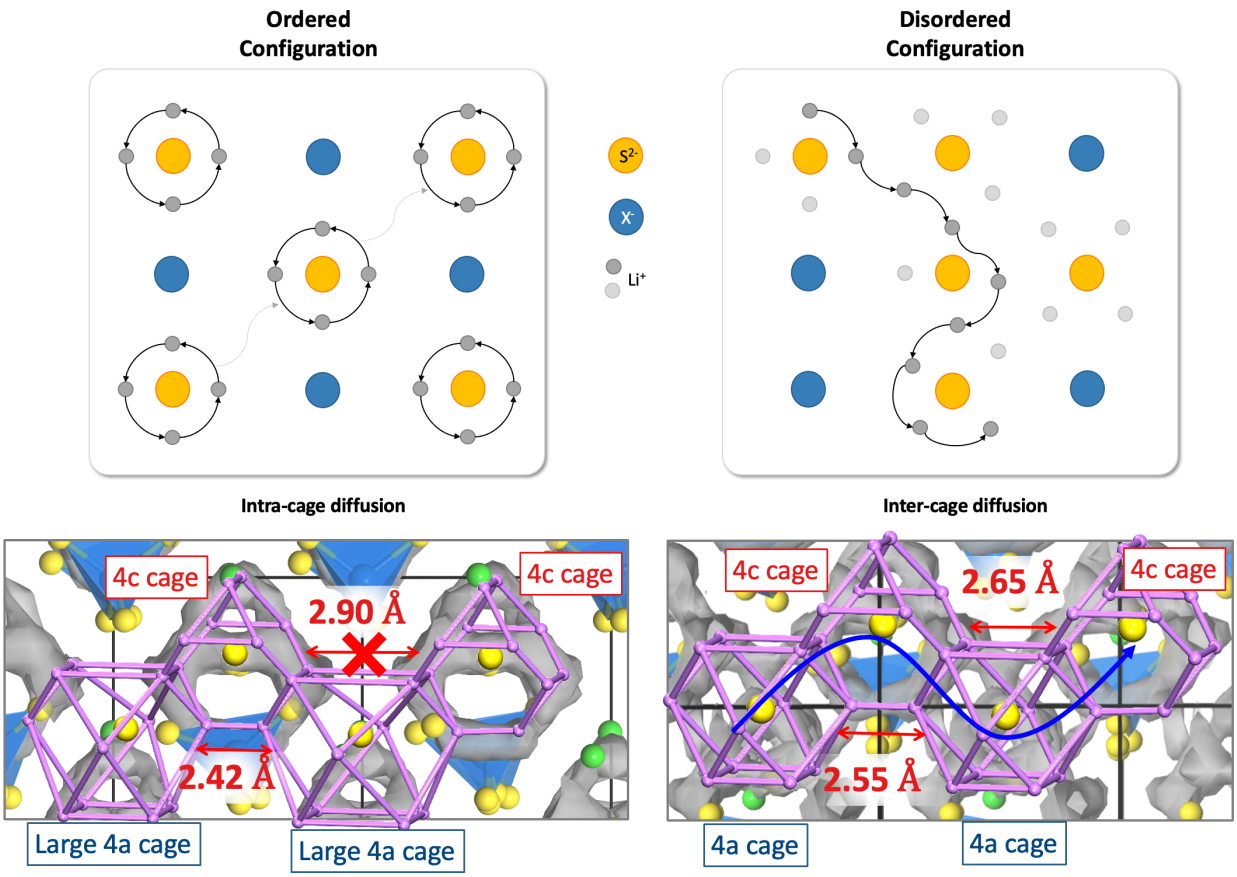

Figure S8. Schematics of intra- and inter-cage diffusion pathway with detailed analysis structures for different site disorder configurations of Li_6PS_5Cl, 100% S^{2-} filled ordered configuration at 4c-sites and 50% site disordered configuration.

References

[1] M.J. Field, P.A. Bash, M. Karplus, *J. Comp.Chem.*, 11 (1990) 700-733.

[2] S. Plimpton, *J. Comp.Phys.*, 117 (1995) 1-19.

[3] R. Iftimie, P. Minary, M.E. Tuckerman, *Proc. Natl. Acad. Sci.,* 102 (2005) 6654-6659.

[4] D. Marx, J. Hutter, Ab initio molecular dynamics: basic theory and advanced methods, Cambridge University Press, (2009).

[5] H. Jónsson, G. Mills, K.W. Jacobsen, Classical and Quantum Dynamics in Condensed Phase Simulations, World Scientific Publishing, (1998) 384-404.

[6] Y. Mo, S.P. Ong, G. Ceder, *Chem. Mater*., 24 (2011) 15-17.

[7] Z. Deng, Z. Zhu, I.-H. Chu, S.P. Ong, *Chemi. Mater.*, 29 (2016) 281-288.

[8] S.P. Ong, Y. Mo, W.D. Richards, L. Miara, H.S. Lee, G. Ceder, *Energy Environ. Sci.*, 6 (2013) 148-156.

[9] Gus L. W. Hart, Rodney W. Forcade, *Phys. Rev. B*, 77 (2008) 224115.

[10] Gus L. W. Hart, Rodney W. Forcade, *Phys. Rev. B*, 80 (2009) 014120

[11] Gus L. W. Hart, Lance J. Nelson, Rodney W. Forcade, *Comp. Mat. Sci.*, 59 (2012) 101-107.

[12] Wiley S. Morgan, Gus L. W. Hart, Rodney W. Forcade, *Comp. Mat. Sci.*, 136 (2017) 144-149.

[13] X. He, Y. Zhu, A. Epstein, Y. Mo, *npj Comp. Mater.*, 4 (2018).

[14] Y. Wang, W.D. Richards, S.P. Ong, L.J. Miara, J.C. Kim, Y. Mo, G. Ceder, *Nature Mater.*, 14 (2015) 1026-1031.

[15] P. Hopkins, A. Fortini, A.J. Archer, M. Schmidt, *J. Chem. Phys.*, 133 (2010) 224505.

[16] S.P. Ong, W.D. Richards, A. Jain, G. Hautier, M. Kocher, S. Cholia, D. Gunter, V.L. Chevrier, K.A. Persson, G. Ceder, *Comp. Mater. Sci.*, 68 (2013) 314-319.

[17] Z. Zhu, I.-H. Chu, Z. Deng, S.P. Ong, *Chem. Mater.*, 27 (2015) 8318-8325.

[18] S. Wang, Q. Bai, A.M. Nolan, Y. Liu, S. Gong, Q. Sun, Y. Mo, *Angew. Chem. Int. Ed. Engl.*, 58 (2019) 8039-8043.

[19] R. Malik, D. Burch, M. Bazant, G. Ceder, *Nano Lett.*, 10 (2010) 4123-4127.

[20] W.D. Jung, J.S. Kim, S. Choi, S. Kim, M. Jeon, H.G. Jung, K.Y. Chung, J.H. Lee, B.K. Kim, J.H. Lee, H. Kim, *Nano Lett.*, 20 (2020) 2303-2309.

[21] P. Adeli, J.D. Bazak, K.H. Park, I. Kochetkov, A. Huq, G.R. Goward, L.F. Nazar, *Angew. Chem. Int. Ed. Engl.*, 58 (2019) 8681-8686.

[22] X. Feng, P.-H. Chien, Y. Wang, S. Patel, P. Wang, H. Liu, M. Immediato-Scuotto, Y.-Y. Hu, *Energy Storage Mater*., 30 (2020) 67-73.